Rare Metal Materials and Engineering
Volume 49, Issue 1, January 2020
Available online at www.rmme.ac.cn

Science Press

Cite this article as: Rare Metal Materials and Engineering, 2020, 49(1): 0116-0124.

ARTICLE

Wear Resistance and Corrosion Resistance of TiO_2-B_4C Composite Coating via Micro-arc Oxidation on Pure Ti

Wang Xian[1], Yu Sirong[1], Zhao Yan[1], Liu Li[1], Liu Enyang[1], Cao Wenan[1], Yuan Ming[2]

[1] China University of Petroleum (East China), Qingdao 266580, China; [2] Ningbo Geely Automobile Research & Development Co., Ltd, Ningbo 315336, China

Abstract: A composite ceramic coating containing B_4C and TiO_2 with excellent wear resistance and corrosion resistance was formed on the pure Ti via micro-arc oxidation. The influence of the concentration of B_4C particles added into electrolyte on the microstructure, phase composition, adhesion, microhardness, roughness, wear resistance and corrosion resistance of the coatings was investigated. The results show that TiO_2-B_4C composite coatings consisting of rutile TiO_2, anatase TiO_2 and B_4C phases were more uniform and denser than TiO_2 coating. With the increase in B_4C particle concentration, the adhesion, the wear resistance and corrosion resistance of the coatings increased firstly and then decreased. TiO_2-0.9B_4C coating displayed the strongest adhesion of 22.6 N due to the most compact microstructure; in addition, it also exhibited the best wear resistance. Its breakage time was 19.24 min and its wear width was 384.53 μm. The wear mechanisms were abrasive wear and fatigue wear. Besides, TiO_2-0.9B_4C coating showed the best corrosion resistance. The self-corrosion potential, polarization resistance and corrosion current density of the coating were −213.38 mV, 5.47×10^4 Ω·cm^2 and 2.37×10^{-6} A cm^{-2}, respectively. According to the Bode-phase diagram, it can be speculated that these coatings were composed of two oxide layers, a porous outer layer and a dense inner layer.

Key words: pure titanium; micro-arc oxidation; B_4C particle; wear; corrosion

Titanium (Ti) and titanium-based alloys are in line with the need of people for health, daily necessities and medical devices due to their high strength to weigh ratio, high corrosion resistance and good biocompatibility[1-6]. Unfortunately, pure Ti has low surface hardness and poor wear resistance, and its corrosion resistance needs to be further improved under harsh conditions[7]. Therefore, it is of great practical significance to obtain a protective coating with excellent wear resistance and corrosion resistance based on the premise of maintaining the high-strength and lightweight properties, for extending the service life of pure Ti. As an effective surface strengthening technology, micro-arc oxidation (MAO) has advantages of easy operation, high efficiency, low cost, and strong adhesion[8,9]. The hardness and wear resistance of the coating prepared by MAO are obviously improved. However, under non-lubrication conditions, the coating exhibits a relatively high friction coefficient[10], and the porous microstructure of the coating greatly affects its corrosion resistance. Therefore, the preparation of a high-density composite ceramic coating by doping with reinforcing particles becomes a key point for solving the problem. Currently, particles that have been studied including graphite[11], MoS_2[12], PTFE[13], Al_2O_3[14], BN[10], SiC[15], etc. However, durability, high-temperature resistance and wear resistance of enhanced coatings still need to be improved. B_4C, known as “black diamond”, has the advantages of low density, high strength, high hardness, high temperature stability, good

Received date: January 25, 2019
Foundation item: the Natural Science Foundation of Shandong Province of China (ZR2017LEM004); the Fundamental Research Funds for the Central Universities (18CX02091A)
Corresponding author: Yu Sirong, Ph. D., Professor, School of Materials Science and Engineering, China University of Petroleum (East China), Qingdao 266580, P. R. China, Tel: 0086-532-86983503-8815, E-mail: yusirongupc@163.com

chemical stability, etc[16-18]. It is often used as wear-resistant material and ceramic reinforcement. In view of its excellent performance, it is speculated that the addition of B_4C particles will improve the wear resistance and corrosion resistance of the coating. Moreover, B_4C particles have been widely used as coating reinforcements, but they have not been studied in enhancing MAO ceramic coating.

In this study, uniform and stable composite ceramic coatings on the surface of pure Ti were prepared via MAO by adding B_4C particles into the electrolyte. The micromorphology, phase composition, wear resistance and corrosion resistance of the coatings were studied. The concentration of B_4C particles was optimized.

1 Experiment

The raw material used for the experiment was pure Ti. The pure Ti was cut into thin slices of 40 mm × 30 mm × 1 mm. The samples were leveled with 240#, 600# and 1000# water sandpaper, cleaned ultrasonically in acetone solution for 30 min, and then dried in warm air.

Different electrolyte systems all contained 10 g/L $NaAlO_2$, 5 g/L NaF and 5 g/L NaOH. A certain quantity of B_4C particles was added into the electrolyte. Samples and the B_4C particle concentration are shown in Table 1. The micromorphology of B_4C particles is shown in Fig.1. The purity of the B_4C particles was 99.9 %.

Before the MAO treatment, the samples needed to be etched for 40 s in HF/HNO_3 solution in the deionized water (2:1:17 volume ratio). The etched samples were then washed in deionized water. The prepared substrates were processed in different electrolyte systems by the WHD-30 pulsed micro-arc oxidation equipment, with current density of 10 A/dm^2, frequency of 400 Hz, and duty cycle of 30 %. Stirring device was used to ensure that the B_4C particles were evenly dispersed in the electrolyte during the test. The treated samples were cleaned ultrasonically in acetone solution for 10 min and then dried. Schematic diagram of micro-arc oxidation is shown in Fig. 2.

Table 1 B_4C particle concentration of samples

Sample	B_4C concentration/g·L^{-1}
TiO_2	0
TiO_2-0.3B_4C	0.3
TiO_2-0.6B_4C	0.6
TiO_2-0.9B_4C	0.9
TiO_2-1.2B_4C	1.2
TiO_2-1.5B_4C	1.5

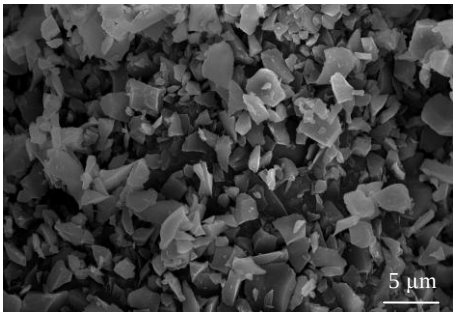

Fig.1 Micromorphology of B_4C particles

The surface micromorphology of the coatings was observed using a scanning electron microscope (SEM: Nova Nano SEM 450) produced by FEI, America. The phase composition was analyzed using X-ray diffraction (XRD: D/MAX-2000) scanning 2θ from 10 ° to 100 ° manufactured by PANalytical BV, Holland. The microhardness was tested using Huayin microhardness tester (HV-1000A), with the pressure of 0.98 N and the holding time of 15 s. The roughness was measured using a confocal microscope (DM2500M). The adhesion was tested using a coating adhesion automatic scratch tester (WS-2005) produced by Lanzhou Zhongke Kaihua Technology Development Company, with a load of 30 N, a loading speed of 30 N/min, and a scratch length of 3 mm. The friction coefficient was tested using controlled atmosphere miniature friction tester (HT-1000), with GCr15 ball as grinding material, a load of 100 g, a rotation speed of 300 r/min, and a rotation radius of 5 mm. The polarization curves and impedance spectra in 3.5 wt% NaCl solution was tested using electrochemical workstation (CS310), with a platinum electrode as the counter electrode and a saturated calomel electrode as the reference electrode.

2 Results and Discussion

2.1 Voltage-time response

Fig.3 shows the voltage-time responses during the MAO treatment in the electrolytes that contained different concentrations of B_4C particles. It was obvious that the responses were characterized by three main stages. At the beginning of the MAO process, the voltage increased linearly with time, referred as anodizing process. A large number of bubbles were generated on the surface of the sample. With the extension of time, the spark discharge stage occurred. The small white sparks to form a pulsed surge were observed on the surface of the sample. Finally, the stage of micro-arc dis-

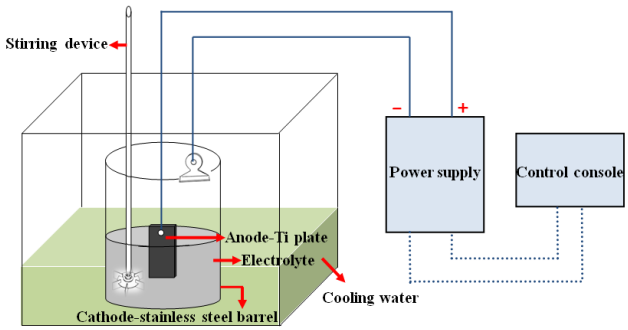

Fig.2 Schematic diagram of micro-arc oxidation

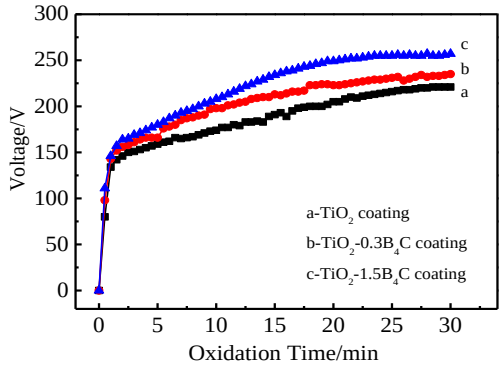

Fig.3 Variation in voltage with MAO treatment time

charge occurred with sharp cracking sound. The voltage was relatively stable in the micro-arc discharge stage. Moreover, with the increase of B_4C particle concentration, the first and second stage time shortened, and the termination voltage and the rate of the voltage increase increased. The addition of B_4C particles was conducive to increase voltage due to the ability to increase the conductivity of the electrolyte.

2.2 Microstructure

Fig.4 shows the microstructures of the TiO_2 coating and TiO_2-B_4C composite coatings. The honeycomb-like and porous structure was observed on all coatings. The micropores were caused by the discharge and the release of bubbles during the breakdown process, and the former played a leading role in the formation of micropores[10]. The porous structure gave the material an ideal surface for mechanical fitting and chemical bonding. If used as an implant material, it can increase the adhesion to the human body and its own biocompatibility[19]. A non-uniform distribution of 0.2 μm to 1.3 μm sized pores was present in the TiO_2 coating, and the size of the pores in the upper part was larger than that in the lower part in Fig. 4a. With the increase in concentration of B_4C particles added in the electrolytes, the surface of the TiO_2-B_4C coatings gradually became smooth, and the micropore radius gradually became small. However, the surface of TiO_2-1.2B_4C coating and TiO_2-1.5B_4C coating became rough. Larger pores, more microcracks and deeper cracks can be seen on these two coatings. In general, the addition of B_4C particles was beneficial to increase the density and pore-uniformity of the coatings, but more addition of B_4C particles was opposite. The reasons were as follows.

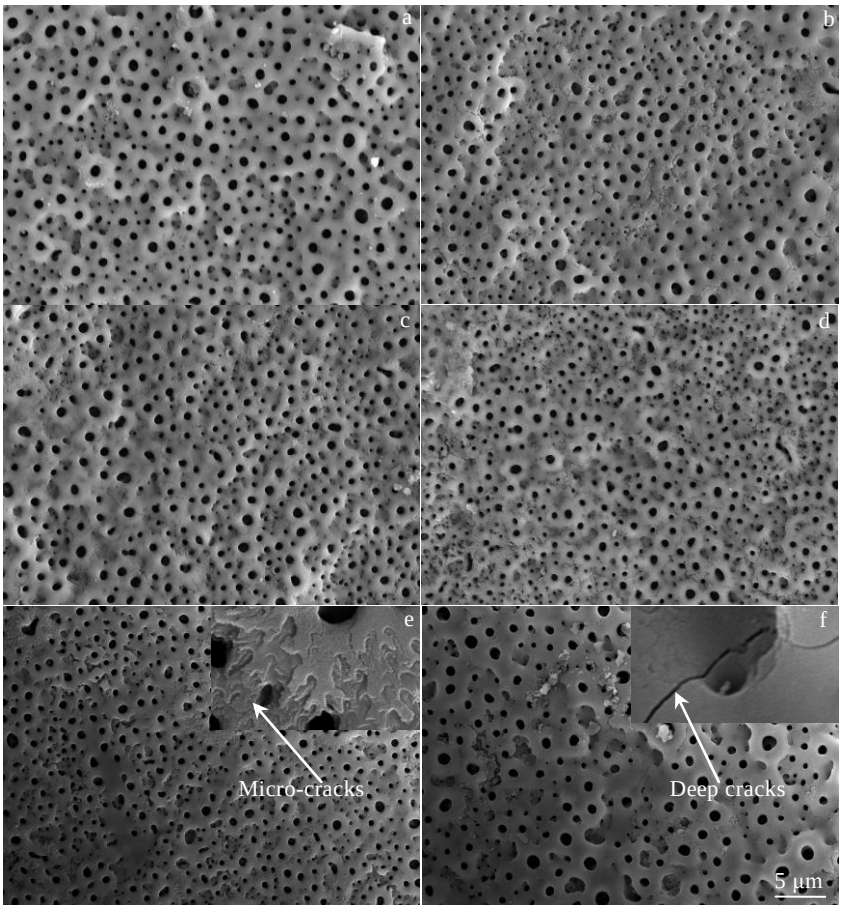

Fig.4 Micromorphology of TiO_2-B_4C coatings: (a) TiO_2, (b) TiO_2-0.3B_4C, (c) TiO_2-0.6B_4C, (d) TiO_2-0.9B_4C, (e) TiO_2-1.2B_4C, and (f) TiO_2-1.5B_4C

On the one hand, the addition of B_4C particles facilitated the increase in the voltage, reduced the arcing voltage and the arcing time, which made the grains small and dense. In addition, the B_4C particles can disperse the current to reduce the local current density, thus making the coatings smooth. On the other hand, B_4C particles entered the coatings through the discharge channel, filling the discharge channel to a certain extent, so that the pore size was reduced[20]. However, when more B_4C particles were added into the electrolyte, the polymerization intensity of coatings weakened due to the excessive voltage, resulting in the decline in quality of coatings.

Fig.5 shows the high magnification micrographs of TiO_2-0.9B_4C composite ceramic coating. It shows that B_4C particles cannot be dissolved or ionized due to their chemically stable structure. B_4C particles were successfully deposited into ceramic coatings during micro-arc oxidation. B_4C particles were mainly concentrated in and near the discharge channels and some were distributed on the surface of ceramic coatings due to physical adsorption.

2.3 Phase composition

Fig.6 shows XRD patterns of the TiO_2 coating and TiO_2-B_4C composite coatings. It can be seen that the TiO_2 coating was composed of rutile TiO_2 and anatase TiO_2, and a new phase B_4C appeared in the TiO_2-0.9B_4C coating and TiO_2-1.5B_4C coating. B_4C had good conductivity and a certain amount of negative charge in the solution. Under the effect of the electric field, B_4C was adsorbed on the surface of pure Ti as the anode and finally entered the coatings by the discharge channel. The difference in concentration between electrolyte and micropores also helped B_4C to enter the coatings.

XRD is produced by the interaction between X-ray and crystalline material. The position of peak represents the diffraction result of X-ray and a crystal plane. The phase can be determined by the position of the peaks. The peak value of XRD is related to crystallinity. Usually, the better the crystallization is, the better the peak shape becomes. In this research, due to high temperature, the crystallization of B_4C might be destroyed during micro-arc oxidation. Therefore, the peak value of B_4C particles changed slightly.

2.4 Microhardness and roughness

Fig.7 shows the microhardness and roughness of pure Ti, the TiO_2 coating and TiO_2-B_4C composite coatings. The microhardness of pure Ti was 1654 MPa. With the increase in B_4C particle concentration, the microhardness of the coatings

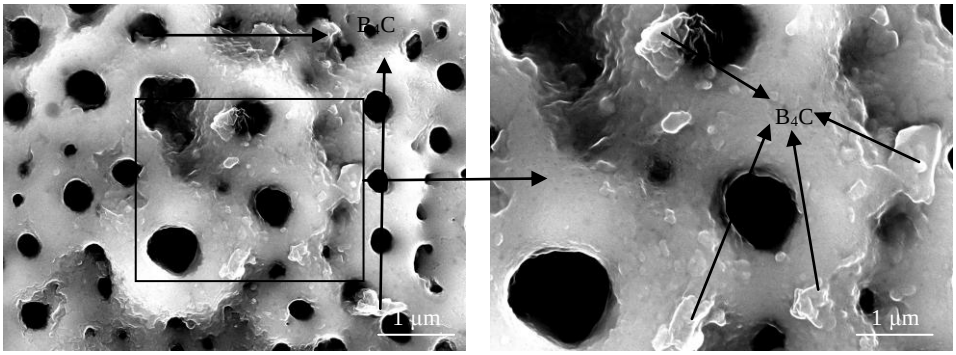

Fig.5 High magnification micrographs of TiO_2-0.9B_4C coating

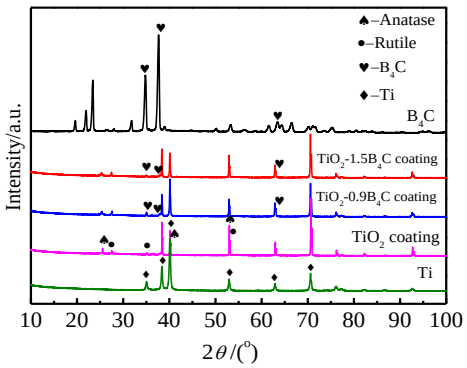

Fig.6 XRD patterns of Ti, B_4C particles, and coatings with different B_4C concentrations

increased firstly and then decreased. The microhardness of the coatings was mainly related to the micromorphology, internal structure, micropore size and uniformity of the coatings. The roughness of pure Ti was 0.3734 μm. The roughness of the coatings was much higher than that of pure Ti. The roughness of the coatings was mainly related to its micromorphology. According to the Griffith and Brichal theory, the lower the porosity is and the more uniform the pores is, the higher the strength of the coatings is. TiO_2-0.9B_4C coating had the highest microhardness HV of 2858 MPa due to the dense and uniform microstructure, thus showing the best quality.

2.5 Adhesion

Fig.8 shows the adhesion of the TiO_2 coating and TiO_2-B_4C composite coatings. Fig. 9 shows the scratch morphology of the coatings. One of the main application re-

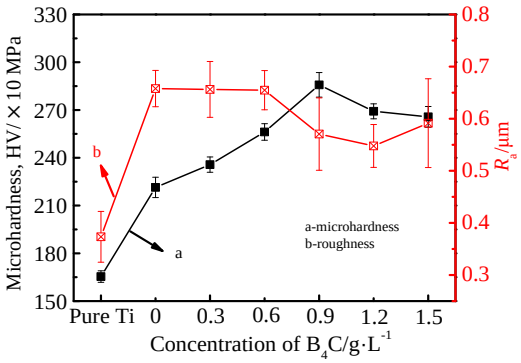

Fig.7 Microhardness HV and roughness R_a of substrate, and coatings with different B_4C concentrations

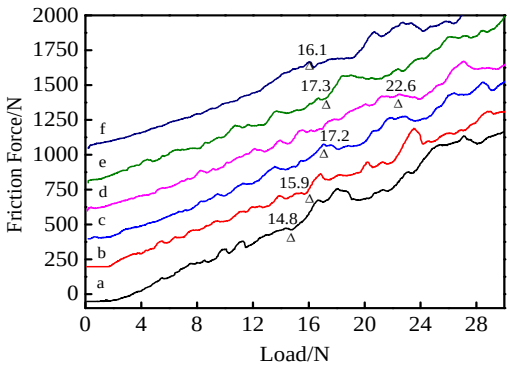

Fig.8 Adhesion of TiO_2 coatings and TiO_2-B_4C composite coatings: (a-TiO_2, b-TiO_2-0.3B_4C, c-TiO_2-0.6B_4C, d-TiO_2-0.9B_4C, e-TiO_2-1.2B_4C, and f-TiO_2-1.5B_4C)

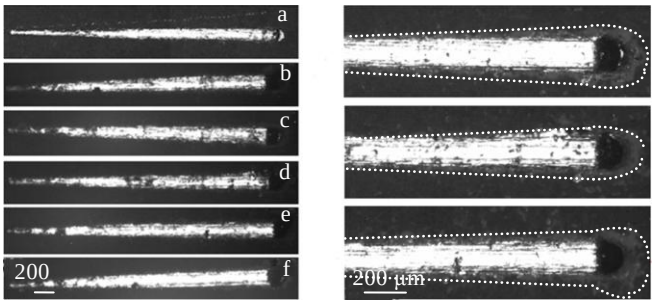

Fig.9 Scratch morphology of TiO_2 coatings and TiO_2-B_4C composite coatings: (a) TiO_2, (b) TiO_2-0.3B_4C, (c) TiO_2-0.6B_4C, (d) TiO_2-0.9B_4C, (e) TiO_2-1.2B_4C, (f) TiO_2-1.5B_4C

quirements for the coatings is to achieve a strong adhesion to the substrate. If adhesion is insufficient, premature failure due to peeling of the coating or formation of microcracks may occur, so it is necessary to study the adhesion between the coatings and the substrate[21]. This experiment adopted the friction detection technology. When the indenter cuts the coating, the load corresponding to the inflection point where the friction coefficient was abrupt was the adhesion of coatings. Due to the porous structure of the ceramic coating, the friction curve will change slightly when the needle scratches through the coating. But when the coating is destroyed or peeled off, the friction coefficient will change greatly. Then, the friction curve will have an obvious inflection point to determine the adhesion of the coating. With the increase in B_4C particle concentration, the adhesion of the coatings gradually increased firstly and then decreased. In Fig.9, in the initial stage of contact between the porous layer of the coatings and the indenter, the scratched surface and the both sides of the coatings were intact. As the load increased, the scratch deepened and widened. Peeling cracks on both sides of the scratch occurred due to the brittleness of the coatings and the strength of the loose layer being lower than that of dense layer[22]. The dashed line represented the boundary of the crack propagation. Compared with other coatings, the TiO_2-0.9B_4C coating had the smallest crack propagation area. It also indicates that the TiO_2-0.9B_4C coating had the strongest adhesion of 22.6 N.

2.6 Wear resistance

Fig.10 shows the friction coefficient and 2 min-wear scar of the TiO_2 coating and TiO_2-B_4C composite coatings. With the increase in B_4C particle concentration, the breakage time of the coatings extended firstly and then shortened, and the wear width was the opposite. TiO_2-0.9B_4C coating had the longest breakage time of 19.24 min and the minimum wear width of 384.53 μm, showing the best wear resistance.

Fig.11 shows the wear scar micromorphology of the TiO_2 coating and TiO_2-B_4C composite coatings. Fig.12 shows the wear mechanism diagram of the coatings. The first contact with the GCr15 ball was the loose layer of the coatings, which only occurred on some convex points. The convex points were peeled off under the action of the cutting force and the pressing force, forming wear debris, which played a role of micro cutting to accelerate the wear of the surface of coatings. Wear debris cannot be removed in time, evolving in abrasive wear. After a period of time, the brittle wear debris was flattened or discharged during the relative motion of the coating. In the sliding wear, the bean-shaped pits appeared in the coatings under the cyclic stress, showing the fatigue wear. When B_4C particles were added, the microhardness of the coatings increased, which hindered the peeling of the microbumps. The wear resistance of the coatings was enhanced due to the self-lubricating feature of the B_4C particles. However, more B_4C particles would affect the growth of the coating, causing the appearance of internal defects and a decline in the quality of the coating, which led to a decrease in wear resistance. TiO_2-0.9B_4C coatings exhibited the best wear resistance due to the highest microhardness and

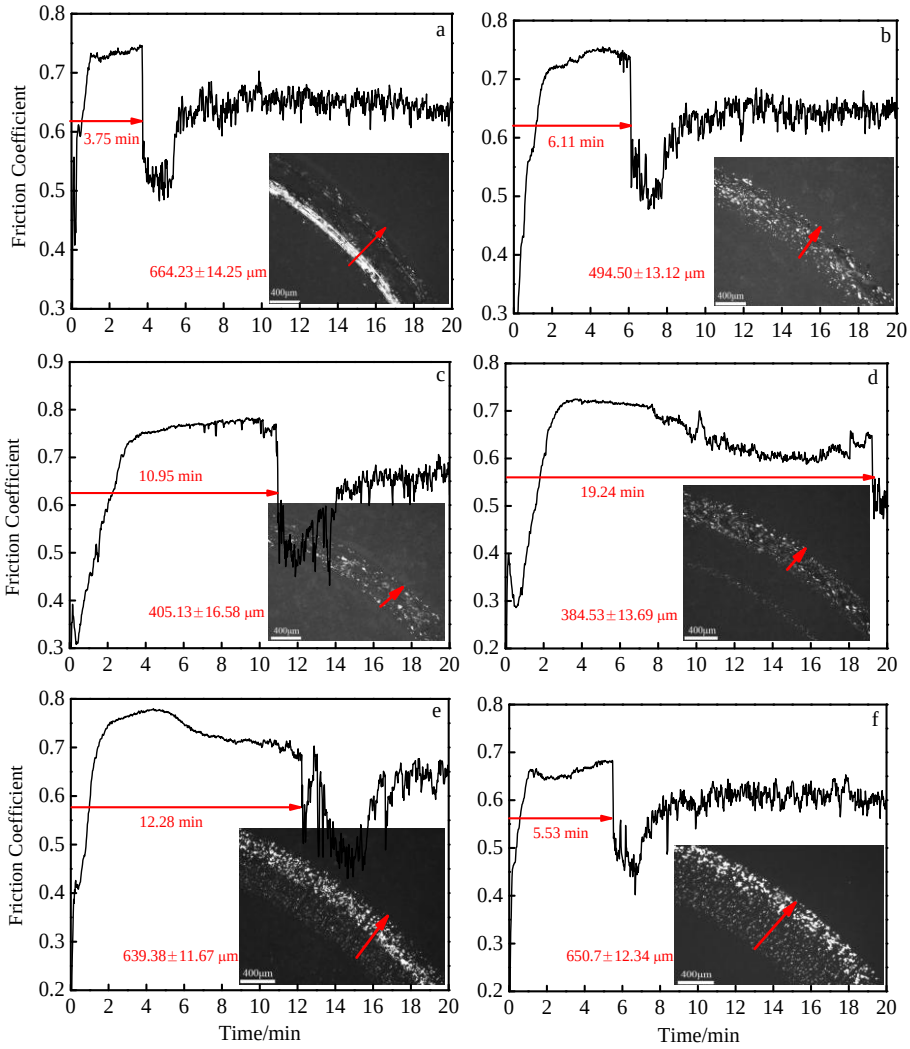

Fig.10 Friction coefficient and 2min-wear scar of coatings with different B_4C concentrations: (a) 0, (b) 0.3B_4C, (c) 0.6B_4C, (d) 0.9B_4C, (e) 1.2B_4C, and (f) 1.5B_4C

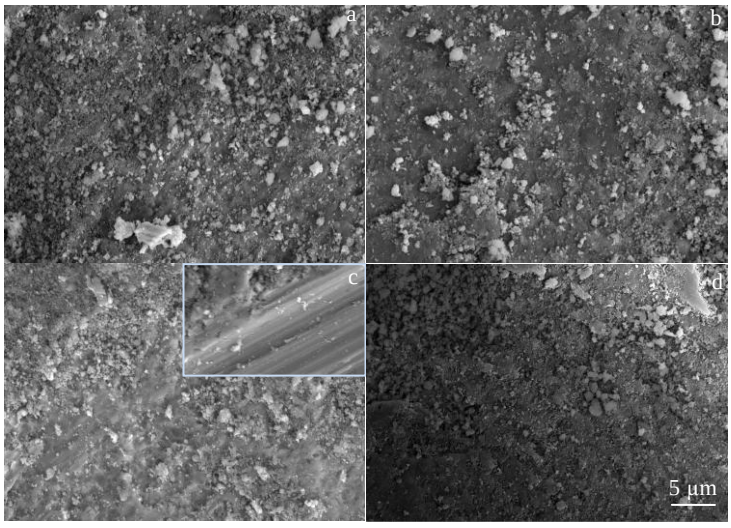

Fig.11 Wear micromorphology of coatings: (a) TiO_2, (b) TiO_2-0.3B_4C, (c) TiO_2-0.9B_4C, and (d) TiO_2-1.2B_4C

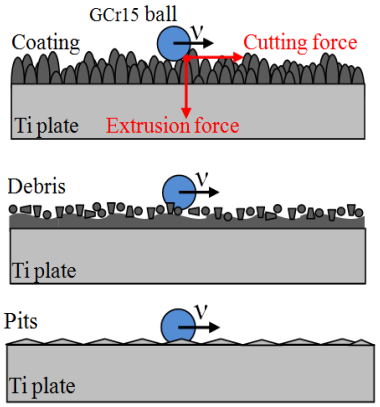

Fig.12 Wear mechanism diagram of TiO_2-B_4C composite coatings

the strongest adhesion. Moreover, the coating close to the wear scar remained intact, indicating that the coating had a strong adhesion.

2.7 Corrosion resistance

Fig.13 shows the polarization curves of the coatings. The electrochemical data is shown in Table 2. During the test, the electrolyte could penetrate to the inside through the swelling of coating and micropores, but the coatings acted as an insulating layer before the electrolyte reached the coating-substrate interface. When the electrolyte reached the coating-substrate interface, it caused corrosion of the substrate, and destroyed the adhesion of the coatings, making the coatings partially deboned or foamed with the substrate. Therefore, it is necessary to study the corrosion resistance of coatings. Compared to substrate, the polarization curve of the coatings moved toward the positive potential and the small current, indicating that the corrosion resistance of the coatings had been significantly improved after MAO treatment. The corrosion resistance of the coatings increased firstly and then decreased with the increase in B_4C particles concentration. TiO_2-$0.9B_4C$ coating exhibited the best corrosion resistance. The self-corrosion potential (E_{corr}) of the coating was −213.38 mV, 58.28% higher than that of substrate. The corrosion current density (I_{corr}) of the coating was 2.37×10^{-6} A cm^{-2}, an order of magnitude lower than that of the substrate. The polarization resistance (P.R.) which was calculated using Stern–Geary equation (Formula (1)) of the coating was 5.47×10^{4} Ω·cm^2, an order of magnitude higher than that of the substrate.

$$\text{P.R.} = \frac{\beta_c\beta_\alpha}{2.303\times(\beta_c\beta_\alpha)}\cdot\frac{1}{I_{corr}} \quad (1)$$

Fig.14 shows the impedance spectra of the TiO_2 coating and TiO_2-B_4C composite coatings. The electrochemical data is shown in Table 3. The radius of the high-frequency capacitance on the Nyquist curve can reflect the charge transfer resistance of the electrode. The larger the radius is,

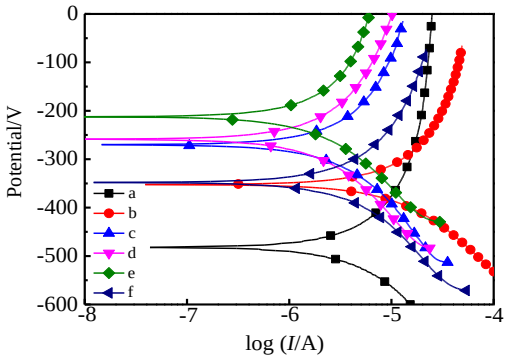

Fig.13 Polarization curves of Ti (a), TiO_2 coating (b), TiO_2-$0.3B_4C$ coating (c), TiO_2-$0.6B_4C$ coating (d), TiO_2-$0.9B_4C$ coating (e), and TiO_2-$1.2B_4C$ coating (f)

Table 2 Electrochemical polarization data of the coatings with different B_4C concentrations

Sample	I_{corr}/ $\times10^{-6}$ A cm^{-2}	E_{corr}/mV	P.R./ $\times10^{4}$ Ω cm^2
Ti	11.76	−488.02	1.29
TiO_2	9.77	−351.698	3.09
TiO_2-$0.3B_4C$	7.79	−272.60	3.38
TiO_2-$0.6B_4C$	2.44	−258.97	3.99
TiO_2-$0.9B_4C$	2.37	−213.38	5.47
TiO_2-$1.2B_4C$	7.95	−350.52	2.42

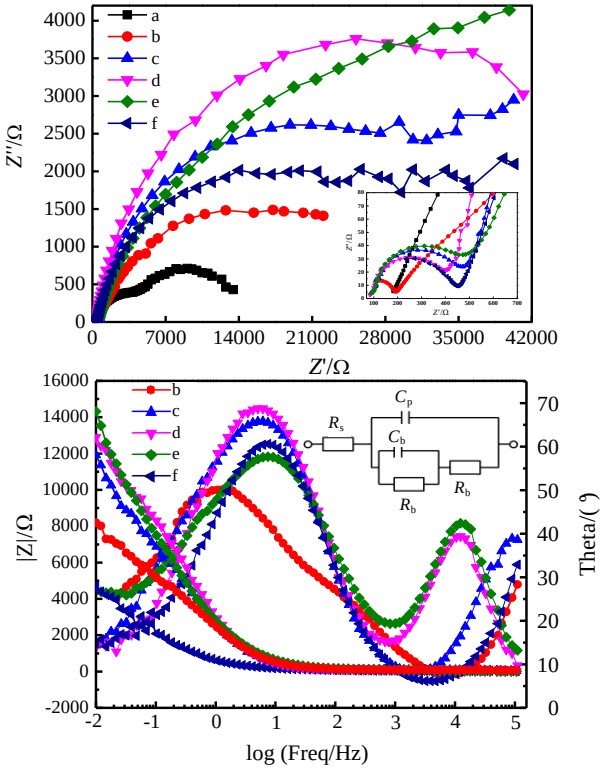

Fig.14 Electrochemical impedance spectra of Ti (a), TiO_2 coating (b), TiO_2-$0.3B_4C$ coating (c), TiO_2-$0.6B_4C$ coating (d), TiO_2-$0.9B_4C$ coating (e), and TiO_2-$1.2B_4C$ coating (f)

Table 3 Electrochemical impedance data of the coatings with different B_4C concentrations

Sample	R_p/Ω·cm^2	R_b/ ×10^4 Ω cm^2	(R_p+R_b)/ ×10^4 Ω·cm^2
TiO_2	299	3.96	3.99
TiO_2-0.3B_4C	324	4.57	4.60
TiO_2-0.6B_4C	319	5.71	5.74
TiO_2-0.9B_4C	340	7.41	7.44
TiO_2-1.2B_4C	344	3.60	3.64

the greater the charge transfer resistance is, and the stronger the corrosion resistance of the coatings is. The trend of the impedance spectra was basically consistent with the polarization curve test results. The Bode-phase diagram showed two time constants, indicating that the coatings consisted of a porous outer layer and a dense inner layer. The first time constant (low frequency band) was related to the dense layer, and the second time constant (high frequency band) was related to the porous outer layer[23]. TiO_2-0.9B_4C coating exhibited the best corrosion resistance, having the largest total resistance (R_p+R_b) of the loose and dense inner layers. The corrosion resistance was mainly related to the density of the coatings and the structure of the micropores.

3 Conclusions

1) TiO_2-B_4C composite coatings consisting of rutile TiO_2, anatase TiO_2 and B_4C phase are more uniform and denser than TiO_2 coating.

2) With the increase in B_4C particle concentration, the microhardness, the adhesion, the wear resistance and the corrosion resistance of the coatings increase firstly and then decrease.

3) TiO_2-0.9B_4C coating exhibits the best comprehensive performance. Its microhardness is 2688 MPa, and its adhesion is 22.6 N. TiO_2-0.9 B_4C coating also has the best wear resistance. Its breakage time is 19.24 min and its wear width is 384.53 μm. The wear mechanisms of these coatings are abrasive wear and fatigue wear. TiO_2-0.9B_4C coating also shows the best corrosion resistance. The self-corrosion potential, polarization resistance and corrosion current density are −213.38 mV, 5.47×10^4 Ω·cm^2 and 2.37×10^{-6} A cm^{-2}, respectively.

References

1 Hsieh S F, Ou S F, Chou C K. *Applied Surface Science*[J], 2017, 392: 581

2 Zhang L, Gao Q, Han Y. *Journal of Materials Science & Technology*[J], 2016, 32(9): 919

3 Feng C J, Hu S L, Jiang Y F *et al*. *Rare Metal Materials and Engineering*[J], 2013, 42(12): 2427 (in Chinese)

4 Khanna R, Kokubo T, Matsushita T *et al*. *Materials Science & Engineering C*[J], 2015, 55: 393

5 Tang W X, Yan J K, Yang G *et al*. *Rare Metal Materials and Engineering*[J], 2014, 43(12): 2883 (in Chinese)

6 Duarte L T, Bolfarini C, Biaggio S R *et al*. *Materials Science & Engineering C*[J], 2014, 41: 343

7 Saleem S, Ahmad R, Ayub R *et al*. *Applied Surface Science*[J], 2017, 394: 586

8 Hong M H, Lee D H, Kim K M *et al*. *Thin Solid Films*[J], 2011, 519(20): 7065

9 Wang J H, Wang J, Lu Y *et al*. *Applied Surface Science*[J], 2015, 324: 405

10 Ni A, Liu D, Wang S *et al*. *Journal of Materials Science & Technology*[J], 2016, 32(10): 1071

11 Tao X W, Yao Z J, Luo X X. *Journal of Alloys & Compounds*[J], 2017, 718: 126

12 Mu M, Liang J, Zhou X *et al*. *Surface & Coatings Technology*[J], 2013, 214: 124

13 Wang Z J, Wu L, Qi Y L *et al*. *Surface & Coating Technology*[J], 2010, 204: 3315

14 Feng J, Dan M, Jin F Y *et al*. *Rare Metal Materials and Engineering* [J], 2016, 45(2): 315 (in Chinese)

15 Wang S Y, Nai-Chao S I, Xia Y P *et al*. *Transactions of Nonferrous Metals Society of China*[J], 2015, 25(6): 1926

16 Adeli R, Shirmardi S P, Ahmadi S J. *Radiation Physics & Chemistry*[J], 2016, 127: 140

17 Aatthisugan I, Rose A R, Jebadurai D S. *Journal of Magnesium & Alloys*[J], 2017, 5(1): 20

18 Shabani M O, Mazahery A, Rahimipour M R *et al*. *Journal of King Saud University-Engineering Sciences*[J], 2012, 24(2): 107

19 Liu Z, Wang W, Liu H *et al*. *Applied Surface Science*[J], 2013, 266(2): 250

20 Yürektürk Y, Muhaffel F, Baydoğan M. *Surface & Coatings Technology*[J], 2015, 269(PR7): 83

21 Moskalewicz T, Kruk A, Kot M *et al*. *Archives of Civil & Mechanical Engineering*[J], 2014, 14(3): 370

22 Gao Yan. *Thesis for Master Degree*[D]. Jiamusi: Jiamusi University, 2014 (in Chinese)

23 Fazel M, Salimijazi H R, Golozar M A *et al*. *Applied Surface Science*[J], 2015, 324: 75

纯钛表面微弧氧化 TiO_2-B_4C 复合陶瓷膜耐磨耐蚀性研究

王 先[1]，于思荣[1]，赵 严[1]，刘 丽[1]，刘恩洋[1]，曹文安[1]，袁 明[2]

(1. 中国石油大学（华东），山东 青岛 266580)

(2. 宁波吉利汽车研究开发有限公司，浙江 宁波 315336)

摘 要：采用微弧氧化工艺，并掺杂 B_4C 颗粒来制备耐磨耐蚀性优异的复合陶瓷膜，系统研究掺杂 B_4C 含量对陶瓷膜微观形貌、物相组成、与基体结合力、显微硬度、粗糙度、耐磨性与耐蚀性的影响。结果表明：相比 TiO_2 陶瓷膜，掺杂 B_4C 颗粒的复合陶瓷膜更均匀致密，且由金红石型 TiO_2、锐钛矿型 TiO_2 和 B_4C 组成。随 B_4C 浓度增大，陶瓷膜的膜层结合力、耐磨性与耐蚀性均先增强后减弱。由于具有最致密的表面形貌，TiO_2-0.9B_4C 复合陶瓷膜的膜层结合力最大，为 22.6 N。TiO_2-0.9B_4C 复合陶瓷膜的破损时间最长，磨痕宽度最小，分别为 19.24 min 和 384.53 μm，耐磨性最好，其磨损机理为磨粒磨损与疲劳磨损。其自腐蚀电位与极化电阻最大，腐蚀电流密度最小，分别为-213.38 mV、$5.47\times10^4\ \Omega\cdot cm^2$ 和 2.37×10^{-6} A cm^{-2}，耐蚀性最好。由 Bode 相图可知，陶瓷膜均由致密内层和疏松表层组成。

关键词：纯钛；微弧氧化；B_4C颗粒；耐磨性；耐蚀性

作者简介：王 先，女，1992 年生，硕士，中国石油大学（华东）材料科学与工程学院，山东 青岛 266580，E-mail: 15763948152@163.com